ISSN 1028-334X, Doklady Earth Sciences, 2022, Vol. 504, Part 2, pp. 403–409. © Pleiades Publishing, Ltd., 2022.
Russian Text © The Author(s), 2022, published in Doklady Rossiiskoi Akademii Nauk. Nauki o Zemle, 2022, Vol. 504, No. 2, pp. 205–212.

GEOECOLOGY

Crystal-Chemical Considerations in the Choice of Matrices for REE-Actinides

Corresponding Member of the RAS S. V. Yudintsev[a,b,*], M. S. Nickolsky[a], O. I. Stefanovsky[b], and B. S. Nikonov[a]

Received March 1, 2022; revised March 9, 2022; accepted March 10, 2022

Abstract—Light rare earth (REE) titanates, such as REE_2TiO_5, $REE_2Ti_2O_7$, and $REE_4Ti_9O_{24}$, are potential matrices for the REE-actinide fraction of high-level waste from the reprocessing of spent nuclear fuel. The data on the "solubility" of impurity elements (zirconium, uranium, and calcium) in these phases are summarized. The structures considered demonstrate limited isomorphism with respect to these elements, according to the reaction $2REE^{3+} = Ca^{2+} + U^{4+}$, which is common for natural minerals and their synthetic analogues. The reasons for the low "solubility" of these impurities in the REE titanates are considered. The role of the crystal-chemical factor in the selection of matrices for the immobilization of the REE-actinide fraction is analyzed.

Keywords: radioactive waste, REE-actinide fraction, immobilization, REE titanates, crystal chemistry
DOI: 10.1134/S1028334X22060150

Russia is implementing two-component nuclear power based on both thermal-neutron and fast-neutron reactors with reprocessing of spent nuclear fuel [1]. Radioactive waste, including high-level waste (HLW), originates from the nuclear fuel cycle. The development of the methods of handling long-lived transuranium actinides (Pu and minor actinides, Np, Am, Cm) is one of the key tasks in improvement of nuclear power safety. Minor actinides can be extracted from the HLW in the form of a REE-MA fraction (MA = Am, Cm) and incorporated in the crystalline phases with low solubility in water for subsequent geological disposal [2]. The REE-MA fraction mostly consist of large lanthanides (La, Ce, Pr, Nd, Sm); Am and Cm account for about 10 wt % [3]. Crystalline REE titanates and zirconates are the most promising matrices for the REE-MA fraction of SPF HLW [1, 2, 4]. Most studies have been devoted to oxides with the structures of pyrochlore and fluorite [2, 4, 5]. Fewer works are available on the properties of the REE titanates. They mainly concern the influence of the REE cations of the structure type of the REE_2TiO_5 and $REE_2Ti_2O_7$ phases and the study of their resistance to ion irradiation [6, 7].

Nd compounds are of great interest in the search for REE-MA matrices because Nd^{3+} is a chemical analogue (imitator) of Am^{3+} and Cm^{3+}. The following phases occur in the Nd_2O_3–TiO_2–ZrO_2 system [8]: pyrochlore $Nd_2(Ti,Zr)_2O_7$ (hereafter, LnTZ), TiO_2 (T, rutile), $ZrTiO_4$ (ZT, shrilankite) and tetragonal ZrO_2 (Z_t). Nd-titanates are represented by Nd_2TiO_5 (LnT), $Nd_2Ti_2O_7$ (LnT_2), $Nd_2Ti_4O_{11}$ (LnT_4), and $Nd_4Ti_9O_{24}$ (Ln_2T_9). Among other REE titanate and zirconate systems, La_2O_3–TiO_2–ZrO_2 [9], Y_2O_3–TiO_2–ZrO_2 [10], and Nd_2O_3–TiO_2 [11] were studied. The identity of $Nd_2Ti_4O_{11}$ and $Nd_4Ti_9O_{24}$ were proven, and the occurrence of $Nd_2Ti_3O_9$ (LnT_3) was established in [11].

The La_2O_3–TiO_2–ZrO_2 system contains the following phases (Fig. 1b): La_2TiO_5 (LnT), $La_4Ti_3O_{12}$ (Ln_2T_3), $La_2Ti_2O_7$ (LnT_2), $La_4Ti_9O_{24}$ (Ln_2T_9), $La_2Zr_2O_7$ (LnZ_2), $ZrTiO_4$ (ZT), ZrO_2 (Z), and TiO_2 (T). The phase sets in the systems with Nd_2O_3 and La_2O_3 are similar. However, the phase relations in the systems considered are different, mostly due to the much smaller area of the La–Zr-pyrochlore (LnZ_2) solid-solution field. Weak variations in the chemical composition are a specific feature of Nd and La titanates. The Ti/REE ratio in the phases is close to stoichiometric values, which is manifested in the narrow stability fields in the diagrams. Less than 2 mol % of ZrO_2 dissolves in the LnT_2, Ln_2T_3, and LnT phases at 1350°C [9], while Ln_2T_9 contains up to 4 mol % of

[a] *Institute of Geology of Ore Deposits, Petrography, Mineralogy, and Geochemistry, Russian Academy of Sciences, Moscow, 119017 Russia*
[b] *Frumkin Institute of Physical Chemistry and Electrochemistry, Russian Academy of Sciences, Moscow, 119991 Russia*
**e-mail: yudintsevsv@gmail.com*

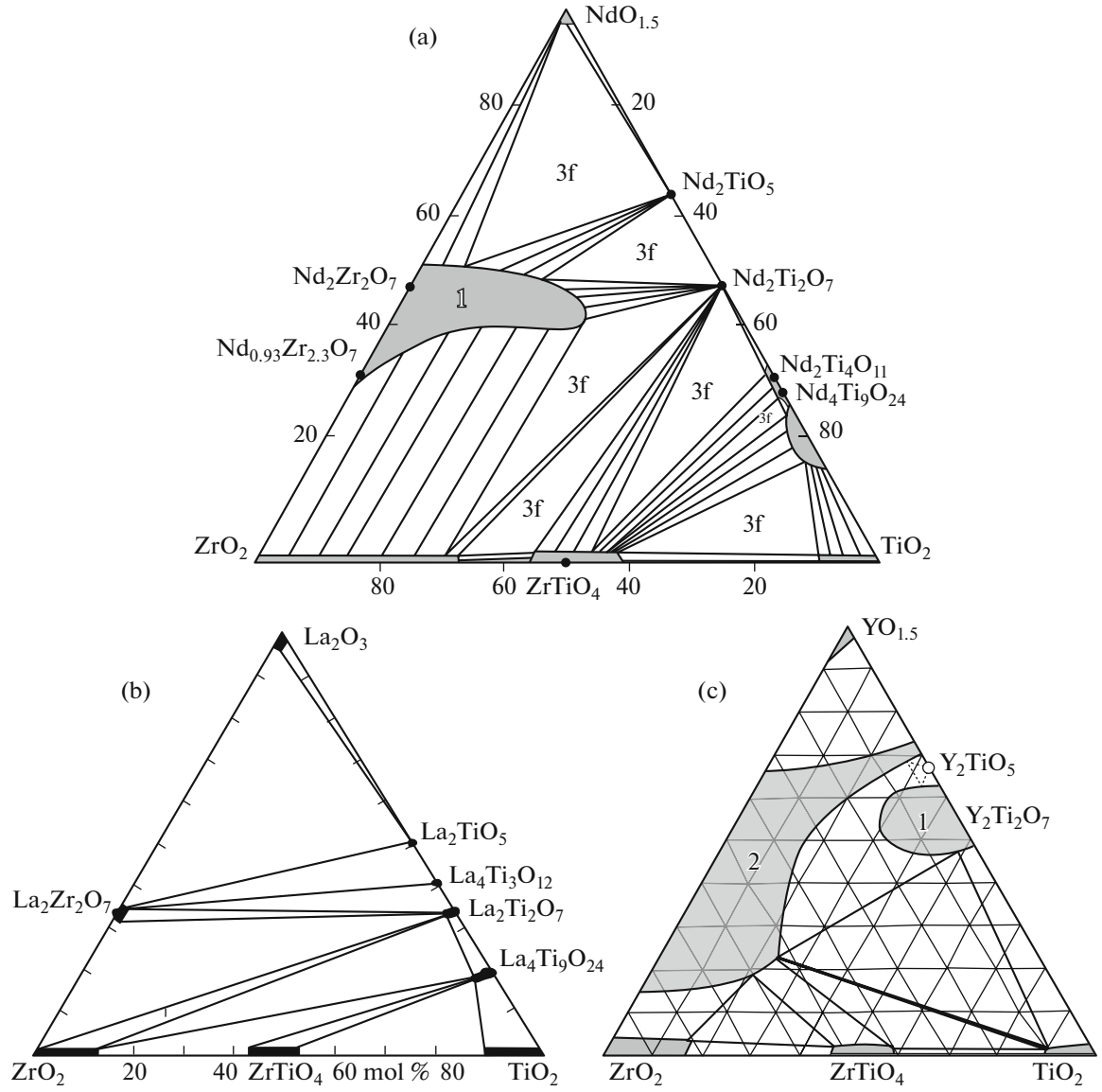

Fig. 1. $NdO_{1.5}$–TiO_2–ZrO_2 (a, 1450°C), La_2O_3–TiO_2–ZrO_2 (b, 1350°C), and $YO_{1.5}$–TiO_2–ZrO_2 (c, 1500°C) systems: 1 and 2, pyrochlore and fluorite fields [8–10].

ZrO_2 (Table 1). $La_2Zr_2O_7$ (LnZ_2) contains up to 35 mol % of La_2O_3 and 69 mol % of ZrO_2, while the ideal stoichiometry suggests 33 and 67 mol % of La_2O_3 and ZrO_2, respectively. Isomorphic substitutions of La^{3+} into ZrO_2 and $ZrTiO_4$ are limited by 1 mol % of La_2O_3. High contents (12–14 mol %) of ZrO_2 in $(Ti,Zr)O_2$ and TiO_2 in $(Zr,Ti)O_2$ were observed. The Zr/Ti ratio in $ZrTiO_4$ varies in a wide range (1.4–0.9). Substitution of large REE^{3+} (La, Nd) for Y^{3+} leads to the transformation of the phase diagram (Fig. 1c). The $Y_2Ti_2O_7$ displays a cubic symmetry (pyrochlore like) and a large solid solution field of $(Zr,Y)O_{2-x}$ fluorite appears in the phase diagram. Oxides TiO_2, ZrO_2, and $ZrTiO_4$ are preserved. The Y_2TiO_5 turns to a cubic modification (sp. group $Fm\bar{3}m$), while Nd_2TiO_5 and La_2TiO_5 belong to the orthorhombic symmetry (sp. group *Pnma*).

Variations of the REE^{3+} radii in the REE_2O_3–TiO_2 and REE_2O_3–ZrO_2 lead to polymorphic transitions. The $REE_2Ti_2O_7$ and $REE_2Zr_2O_7$ compounds form three structure types—fluorite, pyrochlore, and perovskite-like monoclinic titanate [3, 5–7]. The pyrochlore stability field falls to the Shannon radii ratio REE/Ti(Zr) from 1.46 to 1.78. Below 1.46 the fluorite structure type is stable, and above 1.79 the perovskite-like structure type is stable. Titanates of heavy REEs ($Ln_2Ti_2O_7$, Ln = Sm–Yb, Y) and zirconates of light REEs ($Ln_2Zr_2O_7$, Ln = La–Gd)

Table 1. Chemical composition of the phases (mol %) in the La_2O_3–TiO_2–ZrO_2 system according to [9]

Phase and its symbol	La_2O_3	TiO_2	ZrO_2
$La_2Ti_2O_7$, LnT_2	32.3 ± 0.3	66.2 ± 0.2	1.5 ± 0.3
	31.7 ± 0.9	67.2 ± 1.0	1.1 + 0.2
$La_4Ti_9O_{24}$, Ln_2T_9	17.7 ± 1.0	81.1 ± 1.1	2.2 + 0.3
	16.7 ± 0.5	78.9 ± 0.6	4.4 ± 0.2
$ZrTiO_4$, ZT	< bdl	53.1 ± 0.4	46.9 ± 0.3
	< bdl	41.6 ± 0.3	58.4 ± 0.3
ZrO_2, Z_t	< bdl	13.5 ± 0.6	86.5 ± 0.7
TiO_2, T	< bdl	88.6 ± 0.5	11.4 ± 0.3

bdl—below detection limit.

belong to the pyrochlore type of structure. The oxide REE_2TiO_5 displays an orthorhombic symmetry (REE = La–Sm), cubic symmetry (REE = Er–Lu, Sc), and hexagonal symmetry (REE = Ho, Y) [7]. The stability of the structure type with respect to the chemical composition is an important property of the matrices. The appearance of a phase with high solubility in water during the synthesis reduces the performance of the matrices. Previously we studied the distribution of the Ca, Zr, and U impurities in the REE titanates [12–16]. The samples were synthesized by cold pressing and sintering (CPS), cold crucible inductive melting (CCIM), and melting in Joule-heated furnace and crystallization (MC) methods. Tables 2–4 and Fig. 2 list the results of our experiments. A new series of U-bearing samples (NTC-1, NTC-2, NTU-4, NTZ-1, NTZ-2, NTZ-3) was studied.

The observed significant variations of the phase chemical compositions with respect to REE^{3+} (Table 3) are due to the fact that lanthanide titanates (Ln^{3+} = La, Ce, Nd) of the same stoichiometry (LnT, LnT_2, Ln_2T_9) are isostructural. However, contrast to the other REE phases (pyrochlore, zirconolite, monazite, brannerite, etc.), titanates have low solubility for tetravalent (U, Zr) and divalent (Ca) elements.

The ZrO_2 content is 2.0 wt % in Ln_2T_9 (sample MPM-2) and 8.5 wt % in rutile. The U content is 1.3 wt % in Ln_2T_9 (Table 3) and is below the detection limit (0.3–0.5 wt %) in LnT and LnT_2 (Tables 3 and 4). The highest contents of U and Zr (>10 wt %) were found in pyrochlore (Table 4). Those peculiarities of the chemical compositions are due to the crystal chemical properties of the phases considered.

REE titanates and zirconates adopt several structure types. In most of the cases, Ti and Zr ions are six coordinated with O ions forming an octahedron. The dominant coordination numbers of large REEs (La–Sm) are VII (monocapped trigonal prism, truncated cube), VIII (cube, distorted cube, bicapped antiprism), and IX (tricapped trigonal prism). With a decrease in the REE^{3+} radii, the occurrence of coordination number VI increases. Description of the crystal structures of Nd^{3+} oxides is given in Table 5 and Fig. 3.

The $Nd_2Zr_2O_7$ belongs to cubic symmetry (Fig. 3a), space group $Fd\bar{3}m$. The unit cell contains eight formula units. The Nd coordination polyhedron is scalenohedron (distorted cube) with six equidistant O ions and two O ions at a larger distance. The Zr ion centers the trigonal antiprism (distorted octahedron). The pyrochlore structure can be considered as the framework of the BO_6 corner-linked octahedra with AX_2 chains filling the interstices of the octahedral framework. The pyrochlore structure is a derivative of the fluorite structure type AO2 (sp. group $Fm\bar{3}m$).

Table 2. Chemical composition, experiment details, and phase composition according to XRD

Sample	Target composition (formula)	Parameters of the run	Main phases
LT2	$La_{0.5}Nd_{1.4}Sm_{0.1}Ti_2O_7$	CPS: 1400°C, 4 h	LnT_2, Ln_2T_9
3b	$Ln_{1.8}Ca_{0.1}U_{0.1}Ti_2O_7$	CCIM: 1600°C, 1 h	LnT_2, UT_2, O
4	$Ln_{3.6}Ca_{0.2}U_{0.2}Ti_9O_{24}$	the same	Ln_2T_9, UT_2, O
MPM-2	$0.5Ln_4Zr_{0.5}Ti_{8.5}O_{24} + 0.5TiO_2$	the same	Ln_2T_9, T
NTC-1	$0.5(Ca_{0.5}NdU_{0.5})ZrTiO_7 + 0.5Nd_2TiO_5$	MC: 1500°C, 1 h	LnZT, O
NTC-2	$(Ca_{0.25}Nd_{1.5}U_{0.25})(Zr_{0.5}Ti_{1.5})O_7$	the same	LnZT, O
NTU-4	$0.95Nd_2TiO_5 + 0.05UO_2$	the same	LnT_2, Ln_2T_9, O
NTZ-1	$0.4Nd_2TiZrO_7 + 0.4Nd_2TiO_5 + 0.2UO_2$	the same	LnZT, LnT_2, O
NTZ-2	$0.4Nd_2TiZrO_7 + 0.4Nd_2Ti_2O_7 + 0.2UO_2$	the same	LnT_2, O
NTZ-3	$0.4Nd_2TiZrO_7 + 0.3Nd_4Ti_9O_{24} + 0.3UO_2$	the same	UT, Ln_2T_9, T

The Ln–REE mixture $La_{0.12} + Ce_{0.25} + Pr_{0.12} + Nd_{0.41} + Sm_{0.07} + Eu_{0.02} + Gd_{0.01}$. Symbols LnT_2 – $Ln_2Ti_2O_7$, Ln_2T_9 – $Ln_4Ti_9O_{24}$, UT_2 brannerite UTi_2O_6, LnZT $(Ln,Ca,U)_2(Zr,Ti)_2O_7$ pyrochlore, O oxide $(Ln,U)O_{2-x}$, T rutile.

Table 3. Chemical compositions of the REE–U samples "3b" and "4"

Oxide, wt %	Sample "3b"			Sample "4"		
	LnT_2	UT_2	$(Ln,U)O_{2-x}$	Ln_2T_9	UT_2	$(Ln,U)O_{2-x}$
CaO	1.2	< bdl	< bdl	0.7	< bdl	0.6
TiO_2	34.2	45.9	< bdl	52.8	44.5	0.9
La_2O_3	8.7	2.4	< bdl	5.9	2.1	3.1
Ce_2O_3	18.3	14.3	16.8	12.2	10.9	18.7
Pr_2O_3	7.2	2.0	3.2	4.8	1.9	2.9
Nd_2O_3	24.7	8.6	12.6	17.2	8.4	11.4
Sm_2O_3	4.7	2.1	4.5	3.4	2.1	2.9
Eu_2O_3	< bdl	< bdl	< bdl	0.8	0.7	1.0
Gd_2O_3	1.0	< bdl	1.2	0.9	1.0	1.5
UO_2	< bdl	24.7	61.7	1.3	28.4	57.0

bdl—below detection limit. Detection level (0.3–0.5 wt %).

Table 4. Normalized compositions (on 100 wt %) of the U-bearing samples.

Sample	Phase	CaO	TiO_2	ZrO_2	Nd_2O_3	UO_2
NTC-1	Pyrochlore	2.5 (*0.17*)*	28.4 (*0.38*)	11.0 (*0.48*)	50.0 (*0.48*)	8.1 (*0.58*)
	$(Nd,Zr,U)O_{2-x}$	< bdl	< bdl	4.1	26.5	69.4
NTC-2	Pyrochlore	2.1	25.6	11.7	49.3	11.3
	$(Nd,Zr,U)O_{2-x}$	< bdl	< bdl	4.6	18.8	76.6
NTU-4	Nd_2TiO_5	< bdl	19.3	< bdl	80.7	< bdl
	$Nd_2Ti_2O_7$	< bdl	32.1	< bdl	67.9	< bdl
	$(Nd,U)O_{2-x}$	< bdl	1.3	61.6	< bdl	37.1
NTZ-1	Pyrochlore	No	12.5	21.8	54.9	9.7
	$Nd_2Ti_2O_7$	No	32.1	< bdl	65.5	1.2
	$(Nd,Zr,U)O_{2-x}$	No	< bdl	6.5	38.9	54.6
NTZ-2	$Nd_2Ti_2O_7$	No	32.3	0.7	66.3	0.7
	$(Nd,Zr,U)O_{2-x}$	No	1.2	9.5	21.8	67.5
	$(U,Nd)TiO_6$	No	41.9	3.4	18.9	35.8
NTZ-3	$(Ti,Zr)O_2$	No	94.7	5.3	< bdl	< bdl
	$Nd_4Ti_9O_{24}$	No	49.5	1.9	46.4	2.2

*, σ value, d.l., detection limit (0.3–0.5 wt %); No, not present in the charge.

Table 5. Crystal-chemical features of the Nd-phases in the Nd_2O_3–TiO_2–ZrO_2 system

Formula	Space group	Structure type	Nd coordination polyhedron type; the figures in brackets are the Nd^{3+} coordination numbers	Ref
$Nd_2Zr_2O_7$	$Fd\bar{3}m$	$Ca_2Nb_2O_7$	Distorted cube (VIII)	[5, 17]
Nd_2TiO_5	*Pnma*	La_2TiO_5	Monocapped trigonal prism (VII)	[18]
$Nd_2Ti_2O_7$	$P12_11$	$La_2Ti_2O_7$	Distorted mono-, bi-, and tricapped trigonal prism	[17]
$Nd_4Ti_9O_{24}$	*Fddd*	$Nd_4Ti_9O_{24}$	Distorted bicapped antiprism–cube–octahedron	[19]

The $Nd_2Ti_2O_7$ crystal structure is a derivative of the perovskite structure (Fig. 3b). The corner linked TiO_6 octahedra form slabs four octahedra thick (~12 Å) along the directions *a* and *b*. The monocapped trigonal prisms NdO_7 are in-between slabs. Tricapped trigonal prisms NdO_9 fill the interstices of the octahedral slabs. Bicapped prisms NdO_8 occur both inside and in-between slabs.

The Nd_2TiO_5 crystal structure (Fig. 3c) comprises a framework of edge-sharing monocapped trigonal prisms LnO_7 and chains of vertex sharing TiO_5 square pyramids along the [010] direction.

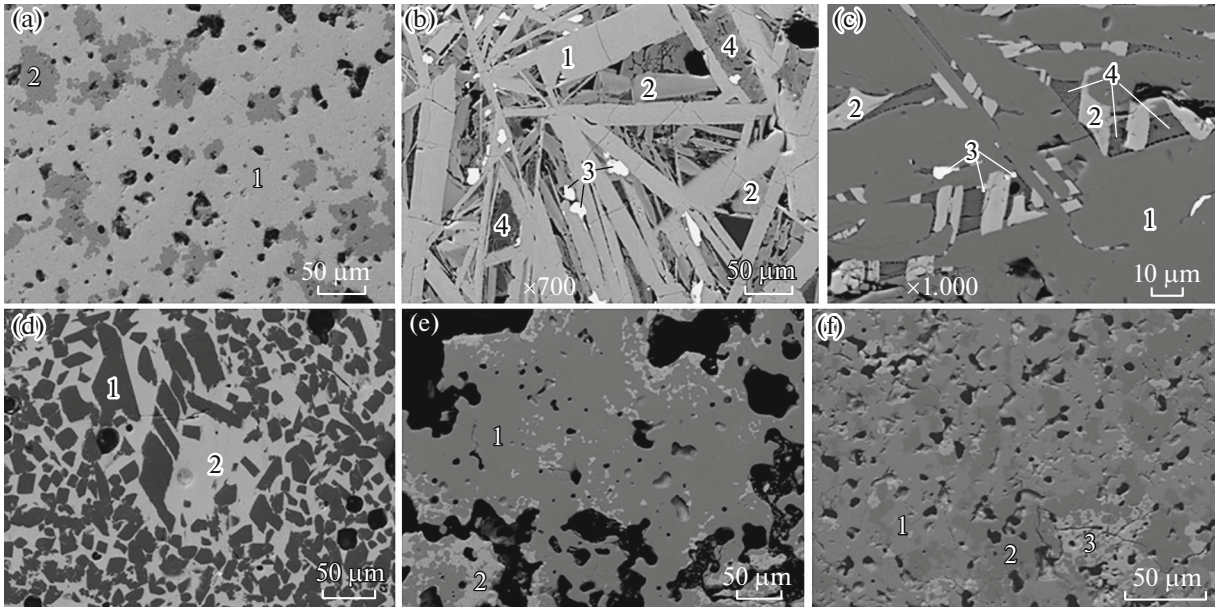

Fig. 2. BSE images of (a) LT2 (1, LnT_2; 2, Ln_2T_9); (b) 3b (1, LnT_2; 2, UT_2, brannerite; 3, $(Ln,U)O_{2-x}$; 4, REE Ti-silicate); (c) 4 (1, Ln_2T_9; 2, UT_2, brannerite; 3, $(Ln,U)O_{2-x}$; 4, REE Ti-silicate); (d); MPM-2 (1, T, rutile; 2, Ln_2T_9), (e) NTC-2 (1, pyrochlore, 2, $(Ln,U)O_{2-x}$); (f) NTU-4 (1, LnT_2; 2, Ln_2T_9; 3, $(Ln,U)O_{2-x}$). Black dots, pores. Scale bar (a, d–f) 50, (b) 20, and (c) 10 microns. The chemical compositions of the phases are listed in Tables 3 and 4.

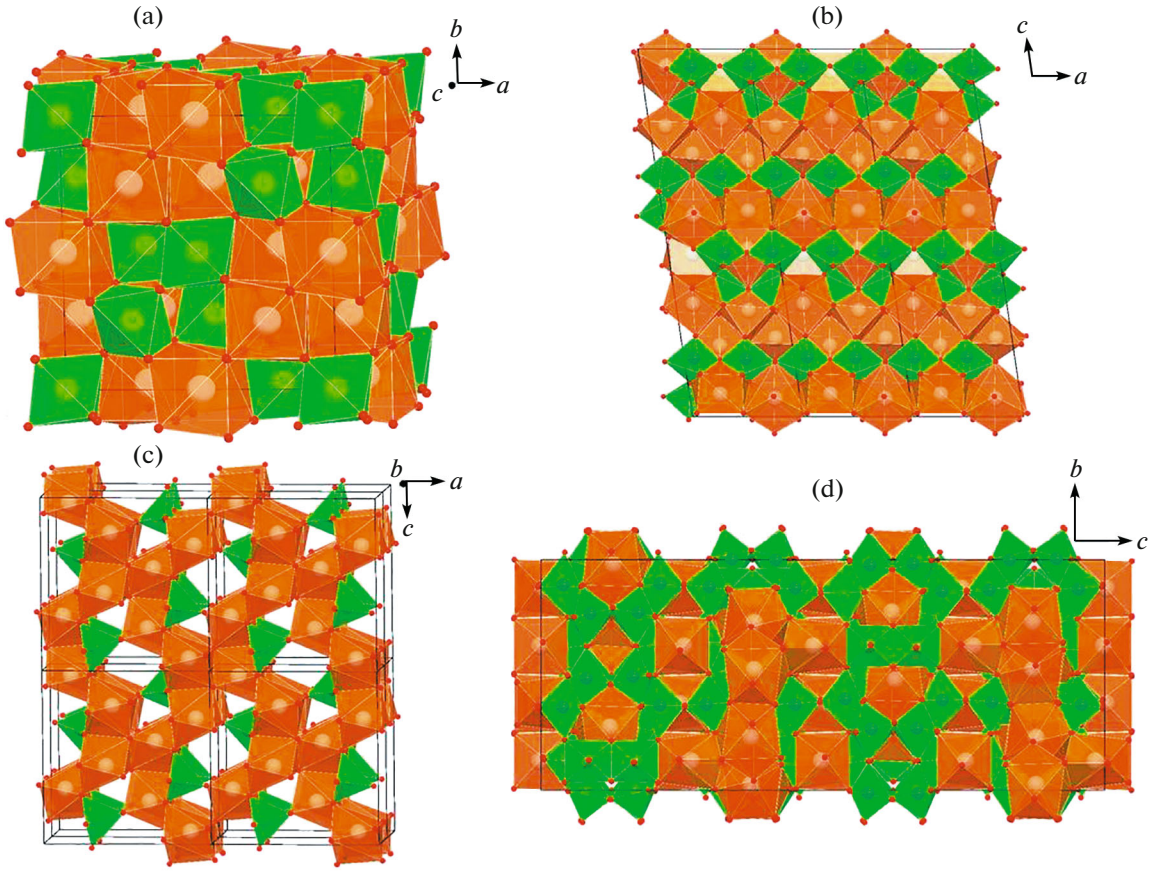

Fig. 3. Crystal structures of the (a) $Nd_2Zr_2O_7$, (b) $Nd_2Ti_2O_7$, (c) Nd_2TiO_5, and (d) $Nd_4Ti_9O_{24}$. Ti and Zr polyhedra are green, and Nd polyhedral are brown.

The $Nd_4Ti_9O_{24}$ oxide has the most complex structure. It consists of a TiO_6 octahedral framework, the cavities of which are filled with Nd ions (Fig. 3d). Nd ions occupy three independent positions in the structure: Nd(1) centers the distorted square antiprism, Nd(2) centers the octahedron, Nd(3) centers a distorted square prism. The $Nd(1)O_8$ polyhedra linked by common vertices and edges form layers parallel to the (110) plane. The Nd(3) polyhedra linked by common edges with Nd(1) layers form complex secondary layers (17.5 Å thick) the cavities of which are filled with isolated Nd(2) octahedra.

The coordination polyhedra of Zr^{4+} and Ti^{4+} are octahedra (coordination number equals VI) in all the phases considered, with the exception of Nd_2TiO_5, where the Ti^{4+} coordination number equals V and the shape of the coordination polyhedron is a square pyramid. This explains the different isomorphism of elements in the phases considered, i.e., a wide field of the pyrochlore solid solution and narrow fields of phases with ratios of elements close to their nominal stoichiometry in other cases. The low solubility of Ca, Zr, and U is typical for the phases with odd Nd coordination numbers (VII and IX). It is worth noting that part of the Nd ions is eight-coordinated in $Nd_4Ti_9O_{24}$. Probably that is the reason for the increased content of U and Zr in $Nd_4Ti_9O_{24}$ relative to $Nd_2Ti_2O_7$ and Nd_2TiO_5.

Narrow stability fields of La^{3+} and Nd^{3+} titanates (Figs. 1a, 1b) contrast with the wide composition variations of pyrochlore, zirconolite, and brannerite, which are also considered as matrices for the REE-actinide fraction. Zirconate and titanium–zirconate pyrochlores have a high isomorphic capacity for actinides in oxidation states other than 3+ [3–5, 20]. The Zr position of pyrochlore $Nd_2Zr_2O_7$ can host up to 20 at. % U, and the Nd position can host from 10 to 20 at. % U and Th. The wide ranges of compositions of zirconolite and brannerite are due to the peculiarities of their crystal structures [3, 4]. Zirconolite $CaZrTi_2O_7$ (Fig. 4a) adopts a monoclinic symmetry (*C*2/*m*), and the Ca and Zr coordination numbers are VIII and VII, respectively. The REE and actinide cations can replace Ca, Zr, and Ti by three mechanisms. The first of them is heterovalent: $Ca^{2+} + Zr^{4+} \rightarrow 2M_1^{3+}$ (M_1 = lanthanides (Ln) and actinides (An)). At a high content of M_1 cations, this structure transforms into $(M_1)_2Ti_2O_7$ pyrochlore. The second variant of heterovalent isomorphism $Ca^{2+} + Ti^{4+} \rightarrow M_1^{3+} + M_2^{3+}$ (M_1 = Ln and An = Pu, Am, Cm; M_2 = Al, Fe). In addition, isovalent substitution of Zr^{4+} for M_3^{4+} cations (M_3 = Ce, An) is possible. In zirconolite, actinides (U, Np, Pu) occur in the Ca and Zr positions in an amount of up to ~0.3 atoms per formula unit. When Zr is completely replaced by actinides, pyrochlore $CaAn^{4+}Ti_2O_7$ is formed. Brannerite crystallizes in a monoclinic symmetry (sp. group *C*2/*m*). The U and Ti cations in the structure of brannerite are located in the centers of octahedra. The TiO_6 octahedra linked by vertices and edges form layers that are parallel to the (001) plane. The columns of UO_6 octahedra going along the *b* axis (Fig. 4b) link the layers together. Large positions are occupied by $(Ce, Th, U, Np, Pu)^{4+}$ or cations of a higher oxidation state (Np^{5+}, U^{5+}/U^{6+}) with simultaneous incorporation of Ca^{2+} and REE^{3+} into the structure to compensate for the charge balance, for example, by the heterovalent scheme: $Ca^{2+} + U^{6+} \rightarrow 2U^{4+}$ or $REE^{3+} + U^{5+} \rightarrow 2U^{4+}$.

CONCLUSIONS

Using the phases of Nd (an imitator of Am and Cm), variations in the composition and crystal chemistry of possible REE-MA matrices in the Nd_2O_3–TiO_2–ZrO_2 system are considered. The system contains, in the order of decrease in the stability fields in the diagram (Fig. 1a), the following phases: $Nd_2(Zr,Ti)_2O_7$, $Nd_4Ti_9O_{24}$, $ZrTiO_4$, $(Zr,Ti)O_2$, $(Ti,Zr)O_2$, $Nd_2Ti_2O_7$, and Nd_2TiO_5. Potential matrices for the REE-MA fraction are $REE_2(Zr,Ti)_2O_{7-x}$ with the pyrochlore structure, $Nd_4Ti_9O_{24}$, $Nd_2Ti_2O_7$ (perovskite), and Nd_2TiO_5. Pyrochlore $Nd_2(Ti,Zr)_2O_7$ has the largest stability field, which includes 10 wt % or more of U and Zr. The "solubility" of Ca, Zr, and U in Nd-titanates is low: from 2–3 wt % in $Nd_4Ti_9O_{24}$ to below the detection limit (0.3–0.5 wt %) in Nd_2TiO_5 and $Nd_2Ti_2O_7$. At an increased content of admixtures, U and REE oxide, U titanate (brannerite), and Ca and Zr titanate (zirconolite) appear in the matrices. The last two compounds are highly stable in solutions, and their appearance will not lead to a deterioration in the insulating properties of matrices with respect to REE-MA. In the REE_2O_3–TiO_2 and REE_2O_3–ZrO_2 systems, as the REE^{3+} radius decreases, the structure of $REE_2Ti_2O_7$ compounds changes from monoclinic perovskite-like to cubic pyrochlore: the polymorphic transition boundary is between Nd and Sm. The $REE_2Zr_2O_7$ phases adopt two related structure types—pyrochlore and fluorite. The first appears at a large difference between the REE^{3+} and Zr^{4+} radii ($R_{REE}/R_{Zr} > 1.46$). As the difference in the ion radii decreases, the pyrochlore structure transforms into an anion-deficient fluorite $(REE, Zr)_4O_7$ structure. The phase transition boundary goes along Gd^{3+}: zirconates of lighter and larger REEs of the Ce group belong to the pyrochlore structure type, while heavy and smaller REEs of the Y group adopt a fluorite-type structure. The situation is more complicated in the case of REE_2TiO_5 compounds: the REE phases from La to Sm adopt an orthorhombic symmetry, from Er to Lu and Sc they have a cubic symmetry, and the REE phases from Eu to Ho and Y are hexagonal.

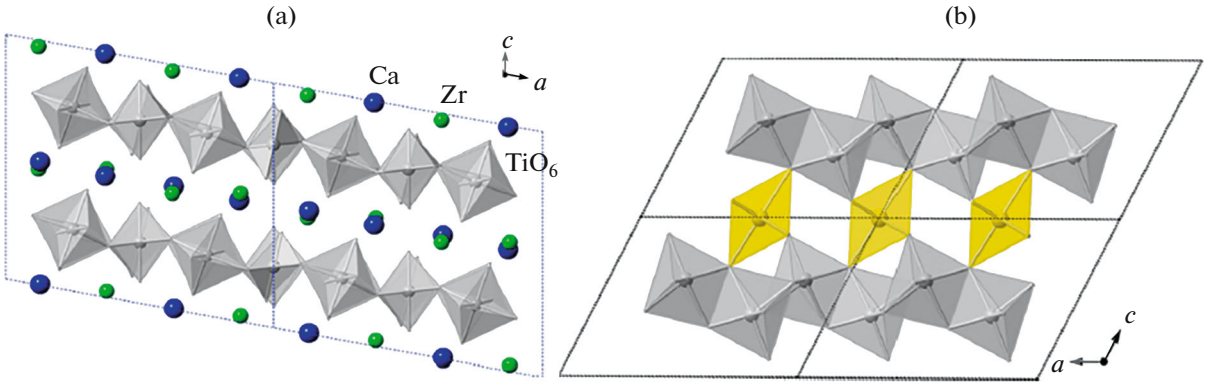

Fig. 4. Crystal structures of (a) zirconolite $CaZrTi_2O_7$ (Ti layers are gray, Ca and Zr atoms are blue and green, respectively) and (b) brannerite UTi_2O_6 (U octahedra (yellow) forms columns parallel to the *b* axis, Ti octahedra (gray) form layers along the (001) plane. U octahedra are linked with Ti octahedra by vertex sharing.

Knowledge of the crystal chemical features of REE phases makes it possible to control the phase composition of the matrices. Admixtures (Zr, Fe, residual amounts of Pu, U) can either be present in the REE-MA fraction or can be specially introduced (CaO, Fe_2O_3, Al_2O_3) into the charge before the matrix is synthesized. As a result, along with REE-MA titanates, it is possible to obtain phases with the structures of pyrochlore, brannerite, and zirconolite, which do not deteriorate the properties of the matrix due to their high corrosion resistance in water.

ACKNOWLEDGMENTS

The authors are grateful to Corresponding Member of the RAS S.V. Krivovichev and an anonymous reviewer for the valuable comments that improved the manuscript significantly.

FUNDING

This work was supported by a State Assignment for the Institute of Geology of Ore Deposits, Petrography, Mineralogy, and Geochemistry, Russian Academy of Sciences.

CONFLICT OF INTEREST

The authors declare that they have no conflicts of interest.

REFERENCES

1. S. V. Yudintsev, Radiochemistry **63** (5), 527–556 (2021).
2. S. V. Stefanovsky and S. V. Yudintsev, Usp. Khim. **85** (9), 962–994 (2016).
3. *Spent Nuclear Fuel Reprocessing Flowsheet* (OECD NEA, Paris, 2012).
4. G. R. Lumpkin, in *Experimental and Theoretical Approaches to Actinide Chemistry,* Ed. by J. K. Gibson and W. A. de Jong (John Wiley & Sons, 2018), Chapter 7, pp. 333–377.
5. R. C. Ewing, W. J. Weber, and J. Lian, J. Appl. Phys. **95** (11), 5949–5971 (2004).
6. K. L. Smith, M. G. Blackford, G. R. Lumpkin, and N. J. Zaluzec, Microsc. Microanal. **12** (2), 1094–1095 (2006).
7. R. D. Aughterson, G. R. Lumpkin, M. Ionescu, M. de los Reyes, B. Gault, K. R. Whittle, K. L. Smith, and J. M. Cairney, J. Nucl. Mater. **467**, 683–691 (2015).
8. S. S. Shoup, C. E. Bamberger, J. L. Tyree, and L. Anovitz, J. Solid-State Chem. **127**, 231–239 (1996).
9. S. D. Skapin, D. Kolar, and D. Suvorov, Solid State Scie. **1**, 245–255 (1999).
10. T. A. Schaedler, O. Fabrichnaya, and C. G. Levi, J. Eur. Ceram. Soc. **28**, 2509–2520 (2008).
11. W. Gong and R. Zhang, J. Alloys Compd. **548**, 216–221 (2013).
12. S. V. Yudintsev, Dokl. Earth Sci. **460** (4), 130–137 (2015).
13. S. V. Yudintsev, S. V. Stefanovsky, M. Yu. Kalenova, B. S. Nikonov, M. S. Nikol'skii, A. M. Koshcheev, and A. S. Shchepin, Radiochemistry **57** (3), 321–334 (2015).
14. S. V. Yudintsev, S. V. Stefanovsky, O. I. Stefanovskaya, B. S. Nikonov, and M. S. Nikol'skii, Radiochemistry **57** (6), 640–652 (2015).
15. S. V. Yudintsev, T. S. Livshits, J. Zhng, and R. C. Ewing, Dokl. Earth Sci. **461** (1), 247–254 (2015).
16. S. V. Yudintsev, M. S. Nikol'skii, B. S. Nikonov, and V. I. Mal'kovskii, Dokl. Earth Sci. **480** (2), 631–637 (2018).
17. E. J. Harvey, K. R. Whittle, G. R. Lumpkin, R. I. Smith, and S. A. T. Redfern, J. Solid State Chem. **178** (3), 800–810 (2005).
18. H. Mueller-Buschbaum and K. Scheunemann, J. Inorg. Nucl. Chem. **35** (4), 1091–1098 (1973).
19. N. Hübner and R. Gruehn, Z. Anorg. Allg. Chem. **616** (10), 86–94 (1992).
20. J. Sun, J. Zhou, Z. Hu, T.-S. Chan, R. Liu, H. Yu, L. Zhang, and J.-Q. Wang, J. Synchrotron. Rad. **29**, 37–44 (2022).

Translated by M.S. Nickolsky